arXiv:2107.08184v1 [nlin.PS] 17 Jul 2021

The Dynamic Scaling Structure of the Intensity–Area–Duration–Frequency Relationship

Victor–Manuel Peñaranda,[1,*] David–Joseph–Auresi Serrano,[2] and Mahesh–Lal Maskey[3]

[1] *Faculty of Engineering and Sciences, Civil Engineering Department, Fundación Universitaria Juan de Castellanos, Tunja, Boyacá, Colombia*
[2] *Department of Civil Engineering, University of Victoria, Victoria BC, Canada*
[3] *Water Systems Management Lab, University of California, Merced, California, USA*

Changing climate signals and the continuous world population growth requires proper hydrologic risk analysis to build and operate water resource infrastructures in a sustainable way. Although modernized computational facilities are becoming popular to understand complex systems, there is not a proper approach for the space – time analysis of extreme rainfall events. Many statistical approaches have been suggested to describe the space–time structure of rainfall; nevertheless, none of them is good enough to represent, for all observational scales, the geometrical structure observed in either rainfall time series or rainfall-derived spatial fields. This research presents a geometric approach to understand the intensity – area – duration – frequency (IADF) relationship without losing information or statistical assumptions. Moreover, this study introduces a promising conceptualization about how understand the space–time structure of rainfall via codimension functions and dynamic scaling theory.

Keywords: rainfall; multifractal; extreme events; probability; IADF relationship; space–time structure, dynamic scaling.

I. INTRODUCTION

Some hydrology applications usually face several kinds of problems related to the analysis of extreme events. The lack of a suitable knowledge of the space–time structure of rainfall at every observational scale represents a challenge when it is necessary to assess the hydrological risk level of a engineering project. The seminal works introduced by Sherman [20] and Bernard [2] suggest to use rainfall intensity–duration–frequency (IDF) curves in order to simplify the complex time structure of rainfall. IDF curves represent a non–linear relationship between the quantities of rainfall intensity, time duration of the rainfall intensity, and the frequency at which the rainfall intensity is expected to happen. The general shape of IDF curves are seen as parallel lines in a logarithmic domain and this shape suggests a mathematical representation of the form [19]:

$$\log i = \log a + b \log T_r - c \log T_d \tag{1}$$

or equivalently:

$$i = \frac{a\, T_r^b}{T_d^c} \tag{2}$$

where i represents the expected rainfall intensity, expressed in mm/hr; T_r is the return period commonly expressed in years; T_d is the duration of the rainfall intensity expressed in minutes; and a, b, c are fitting parameters. There exists several approaches for the construction of IDF curves, however, some difficulties arise in the estimation of their parameters. One of them is the return period T_r which depends on the length of available rainfall records and normally the scale for these available records is the daily scale. The aforementioned establishes controversies for the prognosis of rainfall intensities at short duration via IDF curves. Commonly, the dependence between the

* Correspondence: vpenaranda@jdc.edu.co

return period T_r and the rainfall intensity i is solved by identifying an extreme-type distribution, however, there is not a consolidated theory that explains how this dependence works but an empirical understanding about it [12]. Although some complex approaches suggest to simulate long and synthetic rainfall time series at high–resolution scales for a better understanding of the aforementioned dependencies, the validation of the IDF curves now depends on the simulation model structure and its parametrizations.

Understanding rainfall goes beyond its time structure. It also implies to involve dependencies over spatial scales where rainfall takes place [16]. Therefore, the provision of a tool whereby the space–time structure of rainfall is having into account, gives a better assessment of impacts achieved by extreme rainfall events. Intensity–Area–Duration–Frequency (IADF) curves are considered as the spatial extension of IDF curves [17] and the tool that includes the space–time structure of rainfall. Generally, IADF curves are understood as the combination of IDF curves with areal reduction factors (ARFs) curves [17], however, de Michele et al. [6, 7] and Castro et al. [3] have introduced holistic approaches to gather quantities of rainfall intensity, frequency, time duration and area in a single mathematical expression. To estimate IADF curves, a high–density network of rain gauges and high–resolution time series of rainfall are required; therefore, some problems arise in the light of the quality of hydro-meteorological measurements over developing countries. Although new technologies for rainfall measurement have been created and implemented in different locations of the world, there still exists scarcity of information and a poor understanding of the space–time structure of rainfall, especially in the tropical region.

This research introduced some ideas about how to take advantage of weather–radar products for a better understanding of the space–time structure of rainfall. Previous works on the study of the IADF relationship have shown how important the dynamic–scaling concept is for quantifying the space–time variability of rainfall [3, 6, 7, 18]. However, dynamic scaling theory prompted to the definition of non–universal scaling exponents which have been computed under empirical methodologies. Here, dynamic scaling also plays a important role in the construction of IADF and it also reveals some typical features of dynamic aggregation processes (e.g. diffusion–limited aggregation) that envision a new comprehension of the space–time structure of rainfall.

II. DATA AND METHODS

This section shows the data, tools and methods that were used for this research. The purpose of this work is to show how the scaling structure of the IADF relationship can be identified in weather–radar products, moreover, to expose some statistical interpretations that help to understand the space–time dynamics of rainfall.

A. Definitions

As seen above, equations 2 shows a logarithmic relationship between the mean return period T_r, the time duration T_d and the rainfall intensity i, and such a relationship is an inherent consequence of the multifractal nature of rainfall [10, 11, 13]. Being $\epsilon_\lambda \equiv i_\lambda$ the rainfall intensity measured at the scale λ, the probability of having $i_\lambda > \lambda^\gamma$ could be defined under the power law $\lambda^{-C(\gamma)}$, where λ is representing a (space/time) resolution, γ is a singularity order and $C(\gamma)$ a codimension function that characterizes the probability distribution function (p.d.f.) of rainfall intensities. This codimension function $C(\gamma)$ is expected to be a monotone convex function; therefore, the exceeding probability of $i_\lambda > \lambda^\gamma$ must be a decreasing function. If i_λ comes from a multifractal process there will be a critical value of the order of moment q_d whereby the statistical moments diverge whilst $q > q_d$, therefore, there should be a critical value of the singularity order γ_d associated to the order of the moment q_d. Hubert et al. [10, 11] have suggested the following expression for the codimension function $C(\gamma)$ when the statistical moments divergence takes place:

$$C(\gamma) = q_d\,\gamma - d\,(q_d - 1) \qquad \text{for} \quad \gamma \geq \gamma_d \tag{3}$$

where d is initially set as the fractal dimension of the (space/time) support in which the rainfall field $\mathbf{R}$ is defined at resolution λ. Equation 3 states that for $\gamma \geq \gamma_d$, the codimension function $C(\gamma)$ becomes linear and there would be an algebraic decays of the probability distribution, therefore, $M^q_{i_\lambda}(\lambda) \to \infty$ [10, 14, 21]. When there is a statistical moments divergence, the logarithm of the probability distribution function of the rainfall intensity i_λ is given by:

$$\log \mathbb{P}_{\mathrm{r}}\{i_\lambda > \lambda^\gamma\} \propto -C(\gamma)\, \log \lambda \qquad \text{for} \quad \gamma \geq \gamma_d \tag{4}$$

Relating equations 3 and 4 is obtained:,

$$\log \mathbb{P}_{\mathrm{r}}\{i_\lambda > S_\lambda\} \propto (d\,(q_d - 1) - q_d\,\gamma)\, \log \lambda \tag{5}$$

$$\propto \left(d\,(q_d - 1) - q_d\, \frac{\log S_\lambda}{\log \lambda}\right) \log \lambda \tag{6}$$

$$\propto d\,(q_d - 1)\, \log \lambda - q_d\, \log S_\lambda \tag{7}$$

where $S_\lambda \approx \lambda^\gamma$ represents a threshold value of rainfall intensity i, therefore the approximation $\log S_\lambda \approx \gamma \log \lambda$ is taken into account at equation 7. Defining the time resolution as $\lambda = 1/T_d$ and the probability of the rainfall intensity as $\mathbb{P}_{\mathrm{r}}\{i_\lambda > S_\lambda\} \propto 1/(\lambda\, T_r)$, then, equation 7 can be re-written as follows:

$$\log S_\lambda \propto d\left(1 - \frac{1}{q_d}\right) \log \lambda - \frac{1}{q_d}\, \log \mathbb{P}_{\mathrm{r}}\{i_\lambda > S_\lambda\} \tag{8}$$

$$\propto d\left(1 - \frac{1}{q_d}\right) \log \lambda + \frac{1}{q_d}\, (\log \lambda + \log T_r) \tag{9}$$

$$\propto \left[\frac{1}{q_d} + d\left(1 - \frac{1}{q_d}\right)\right] \log \lambda + \frac{1}{q_d}\, \log T_r \tag{10}$$

$$\propto \left[\frac{1}{q_d} + d\left(1 - \frac{1}{q_d}\right)\right] (-\log T_d) + \frac{1}{q_d}\, \log T_r \tag{11}$$

$$\approx C_o + \frac{1}{q_d}\, \log T_r - \left[\frac{1}{q_d} + d\left(1 - \frac{1}{q_d}\right)\right] \log T_d \tag{12}$$

where C_o is a proportionality factor. Comparing equations 2 and 12, the parameters of the IDF–curves estimation model are obtained as follows:

$$\log a = C_o; \tag{13}$$

$$b = \frac{1}{q_d}; \tag{14}$$

$$c = \frac{1}{q_d} + d\left(1 - \frac{1}{q_d}\right) \tag{15}$$

Therefore, the IDF relationship would be given by:

$$S_\lambda = C_o\, \left[\frac{T_r}{T_d^{1+d\,(q_d - 1)}}\right]^{\frac{1}{q_d}} \tag{16}$$

Equations 13 to 15 exhibit the scaling properties of the IDF relationship through the geometrical analysis of the codimension function $C(\gamma)$.

B. Dynamic Scaling Hypothesis

Some non-equilibrium physical processes exhibit growth processes, for instance: aggregation, nucleation, coagulation, floculation, polymerization an so on. Rainfall could also be described

as a dynamic growth process of clusters at different spatial scales. Diffusion–limited aggregation (DLA) models are used for describing dynamic growth processes; for instance, Vicsek and Family [26] studied the cluster size distribution in a DLA model to get a space–time description of such clusters. Similarly, if rainfall keeps resemblances with dynamic growth processes, it is feasible to think that there should be a dynamic scaling function for the space–time description of rainfall intensity fields.

Based on the aforementioned, during the space–time evolution of the rainfall intensity field $i(x, y, t)$, there exist rain–clusters of area $A_i(t)$ with spatially-averaged rainfall intensity i. If the rain–clusters distribution $f_i(A_i(t))$ follows a dynamic scaling there will be a scaling function of the form:

$$f_i(A_i(t)) \propto A_i(t)^m \Phi\left(\frac{A_i(t)}{t^z}\right) \tag{17}$$

where m and z are dynamic scaling exponents of the rainfall intensity field and $\Phi(\cdot)$ is a scaling function. A physical interpretation of equation 17 can be understood in similar way to that given in growth processes [8, 23, 26]; it means that smaller clusters vanish to give rise to larger clusters (i.e. aggregation), and smaller clusters are those that have the most intense rainfall and they evolve to larger and less intense clusters. Considering there is a dynamic dependence among the cluster area and time, the dynamic scaling exponent z could be computed through the following relationship:

$$A_i(t) \propto t^z \tag{18}$$

Equation 18 suggest that as time goes the rainfall field tends to be more uniform in the space, therefore, the rain cluster areas grows up to reach a quasi–steady state into the atmospheric environment.

C. Data

TRMM–LBA S-POL space–time rainfall intensity records were the weather–radar product that was used for the research purposes. The TRMM–LBA[1] experiment was carried out in the Amazonia from November 1st of 1998 to February 28th of 1999 with the objective of understanding the physical and dynamical characteristics of the tropical rainfall over the Amazonia. The rainfall intensity data are available as compressed ascii files with the following format: $\{x, y, rr, \text{method}\}$, where x, y are relative coordinates to the S-POL[2] origin and they are expressed in kilometers, rr is the rainfall intensity value expressed in mm hr^{-1}, and method is the technique that was used to compute the rain rate. The spatial resolution is 2 km over an observational range of 100 km, the time resolution of the S-POL data spanning between 7 and 10 minutes, and the observation window start in January 10th to February 28th of 1999. Figures 1 and 2 illustrate the main statistical features of the studied rainfall field. Figure 1 shows the time–averaged rainfall intensity field and Figure 2 shows the rainfall intensity variability over the observational range. As shown in Figures 1 and 2, there is a highly complex space–time structure of the amazonian rainfall.

D. Space–Time Codimension Function

S-POL rainfall intensity data were analyzed over time and space, independently. S-POL rainfall intensity fields are over a circular domain where every point $\{x, y\}$ belonging to the spatial field of

---

[1] TRMM: Tropical Rainfall Measurement Mission. LBA: Large Scale Biosphere–Atmosphere Experiment in Amazonia

[2] S-POL refers to a S–band (11 cm) dual–polarimetric radar.

the rainfall intensity, possesses an observation of rainfall intensity $i(x, y)$ at time t, therefore, for the estimation of the codimension function, the distribution of spatial singularities of rainfall–intensity γ_s can be computed as follows:

$$\Pr\{i_\lambda(x, y, t) \geq \lambda_s^\gamma\} \propto \lambda_s^{-C_s(\gamma)} \qquad \text{for} \quad t = t^* \tag{19}$$

where λ_s is the spatial resolution of the S-POL rainfall intensity data and $C_s(\gamma_s)$ is the spatial codimension function. Likewise, the distribution of time singularities γ_t can be computed as follows:

$$\Pr\{i_\lambda(x, y, t) \geq \lambda_t^\gamma\} \propto \lambda_t^{-C_t(\gamma)} \qquad \text{for} \quad x = x^*;\, y = y^* \tag{20}$$

where λ_t is the time resolution of the S-POL rainfall intensity data, $C_t(\gamma_t)$ is the time codimension function and $\Pr\{i_\lambda(x, y, t) \geq \lambda_t^\gamma\}$ is the exceeding probability distribution.

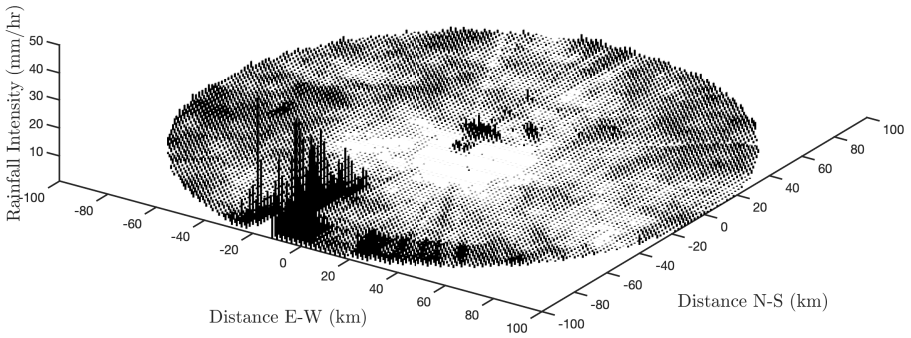


FIG. 1. Time–averaged rainfall intensity field obtained from the S-POL Radar data. The average field was computed for measured the fields between January 10th of 1999 to February 28th of 1999.

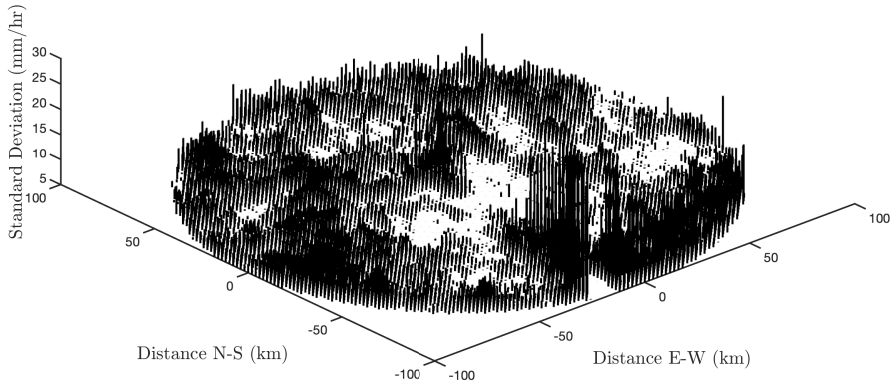


FIG. 2. Standard deviation field for the rainfall intensity fields measured by the S-POL Radar. The standard deviation field was computed for the measured rainfall fields between January 10th of 1999 to February 28th of 1999.

Equations 19 and 20 represent measures of a probability space which space–time singularities orders are the key for understanding the rainfall dynamics [14]. It is highlighted that for every

S–POL rainfall–intensity data-set is selected a collection of N_s observations which satisfy that $\{i(x,y,t)\}_{N_s} > 0$, thus the sampling dimension D_0 is computed as follows:

$$D_0 = \frac{\log N_s}{\log \lambda} \tag{21}$$

Among the properties of the codimension function $C(\gamma)$, it is highlighted that $C(\gamma)$ is an increasing and convex function of the singularities γ, therefore, $dC(\gamma)/d\gamma > 0$ and $d^2C(\gamma)/d\gamma^2 > 0$, respectively. Another property to take into account is the divergence of statistical moments (i.e. $M_\epsilon^q(\lambda) \to \infty$) such as there exists a critical value $q_c \in q$ when γ^+ exceeds the embedding dimension d [14, 21]. The divergence of statistical moments $M_\epsilon^q(\lambda) \to \infty$ at $q \geq q_c$ can be also understood through the codimension function $C(\gamma)$ [24]. A linear behavior of $C(\gamma)$ implies a power–law tail on the probability distribution $\mathbb{P}_\mathrm{r}\{\epsilon_\lambda > s\} \sim s^{-q_c}$ for a large enough threshold s. When a power–law probability distribution is identified in geophysical records, there could be a signature of a possible *self-organized criticality process* [14], i.e. rare (or singular) events play an important role in the data statistical organization. Since there could be a statistical moment divergence in the rainfall intensity distribution, the codimension function will follow a linear form:

$$C(\gamma) = q_d(\gamma - d) + d \qquad \text{for} \quad \gamma \geq \gamma_d \tag{22}$$

or equivalently,

$$C(\gamma) = q_d\gamma - d(q_d - 1) \qquad \text{for} \quad \gamma \geq \gamma_d \tag{23}$$

This linear form of the codimension function implies there is a power–law tail on the probability distribution. A linear regression analysis in the relationship between the codimension function $C(\gamma)$ and the singularity order γ was employed for finding the values of q_d and d. The empirical form of the codimension function $C(\gamma)$ was also studied via non–linear regression analysis. Among the mathematical approximations for the representation of the codimension function $C(\gamma)$, the exponential and power fitting were used. At table I is shown the mathematical expressions for every non–linear fitting method.

TABLE I. This is a table caption. Tables should be placed in the main text near to the first time they are cited.

Fitting Method	**Mathematical Form**	**Coefficients**
Exponential	$C(\gamma) = c_1\, e^{c_2\gamma} + c_3\, e^{c_4\gamma}$	c_1, c_2, c_3, c_4
Power	$C(\gamma) = c_1\, \gamma^{c_2} + c_3$	c_1, c_2, c_3

E. Definition of Cluster Areas

For the definition of cluster areas with a specific value of rainfall intensity i, the Davies–Bouldin index (DBI) [5] was adopted in this work as a cluster separation criteria. Every rainfall intensity field is formed by members $i(x,y)$ at time t, and every cluster C is formed by the subset of punctual rainfall intensity values $\{i_k(x,y)\}_C$ which spatial dispersion measure $S_c(i_1(x,y), i_1(x,y), \ldots, i_k(x,y))$ is defined as:

$$S_c = \left[\frac{1}{T_c}\sum_{j=1}^{T_c} |i_k(x,y) - C_c|^q\right]^{1/q} \tag{24}$$

where T_c is the number of vectors in cluster C and C_c is the centroid of cluster C. The cluster similarity measure $R_{m,n}(S_m, S_n, M_{m,n})$ is defined as follows:

$$R_{m,n} = \frac{S_m + S_n}{M_{m,n}} \tag{25}$$

where $M_{m,n}$ is the distance between vector which are selected as belonging to clusters m and n, therefore, its formal definition is given by:

$$M_{m,n} = \left[\sum_{k=1}^{N} |a_m^{(k)} - a_n^{(k)}|^p \right]^{1/p} \tag{26}$$

where $a_m^{(k)}$ is the k-th component of the vector a_m which is the centroid of the cluster m. The value of the exponent p that was taken for our algorithm equals 2 that representing an Euclidean distance in equation 26. On the other hand, the value of the exponent q is also equal to 2 that representing the standard deviation of the distance of samples in a cluster respect to its centroid. Based on the aforementioned, DBI is defined as:

$$\text{DBI} = \frac{1}{N} \sum_{i=1}^{N} \max\{R_{i,j}\} \qquad \text{for} \quad i \neq j \tag{27}$$

where N is the number of clusters and DBI is representing an average of similarity measures of each cluster with its most similar cluster. Once the number of elements per cluster n_c is defined, the area of every cluster A is computed as follows:

$$A_c = \ell^2 \, n_c \tag{28}$$

where A_c is the area of the cluster C and $\ell \equiv 2$ km^2 is the spatial scale of the S–POL rainfall intensity field.

III. RESULTS

A. Space–Time Codimension Functions

The space–time scaling properties of the S–POL rainfall–intensity dataset were studied through the analysis of the codimension function $C(\gamma)$. Figures 3 and 4 show the space–time codimension functions classified according to percentiles of the sampling dimension D_0. Previously to the estimation of the codimension function, it was necessary to define a classification criteria to ease the statistical analysis of results. For every rainfall intensity field was computed its sampling dimension D_0, the average rainfall intensity $\langle i(x,y,t) \rangle$ and the standard deviation of rainfall intensity field $\text{var}\{i(x,y,t)\}$. A summary of those results are exhibited at tables II and III.

For the spatial domain the sampling dimension D_0 ranges between 0.52 to 1.78 and its average value is $\overline{D_0} = 1.23$. It is observed that the spatial sampling dimension D_0 is highly dynamic in time, thus it can be considered a state variable of rainfall processes. As observed in table II, higher values of D_0 represent higher intensity of the rainfall field, generally. However, those fields classified in percentiles 60 and 70 exhibit statistical differences to other results as be the highest variability and average quantity of rainfall intensity. Figure 3 shows spatial codimension functions which are classified according to percentiles of the sampling dimensions D_0; moreover, in every plot of the codimension function is identified an exponential fitting (in continuous black lines) and the codimension function slope (in dashed red line) when there is a divergence of the statistical moments.

TABLE II. Estimations of the spatial sampling dimension D_0, the average rainfall intensity $\langle i(x,y,t) \rangle$ and the standard deviation of rainfall intensity field $\text{var}\{i(x,y,t)\}$ for the S-POL rainfall intensity fields. These estimations are classified by percentiles of the sampling dimension D_0 of every rainfall intensity dataset.

Percentil	**10**	**20**	**30**	**40**	**50**	**60**	**70**	**80**	**90**	**100**
D_0	0.848	1.013	1.127	1.202	1.272	1.335	1.395	1.456	1.514	1.778
$\langle i(x,y,t) \rangle$	0.844	1.451	1.888	1.615	2.026	2.282	2.882	1.763	2.384	2.708
$\text{var}\{i(x,y,t)\}$	3.209	5.067	5.680	4.754	5.631	7.055	8.101	4.754	5.862	6.094

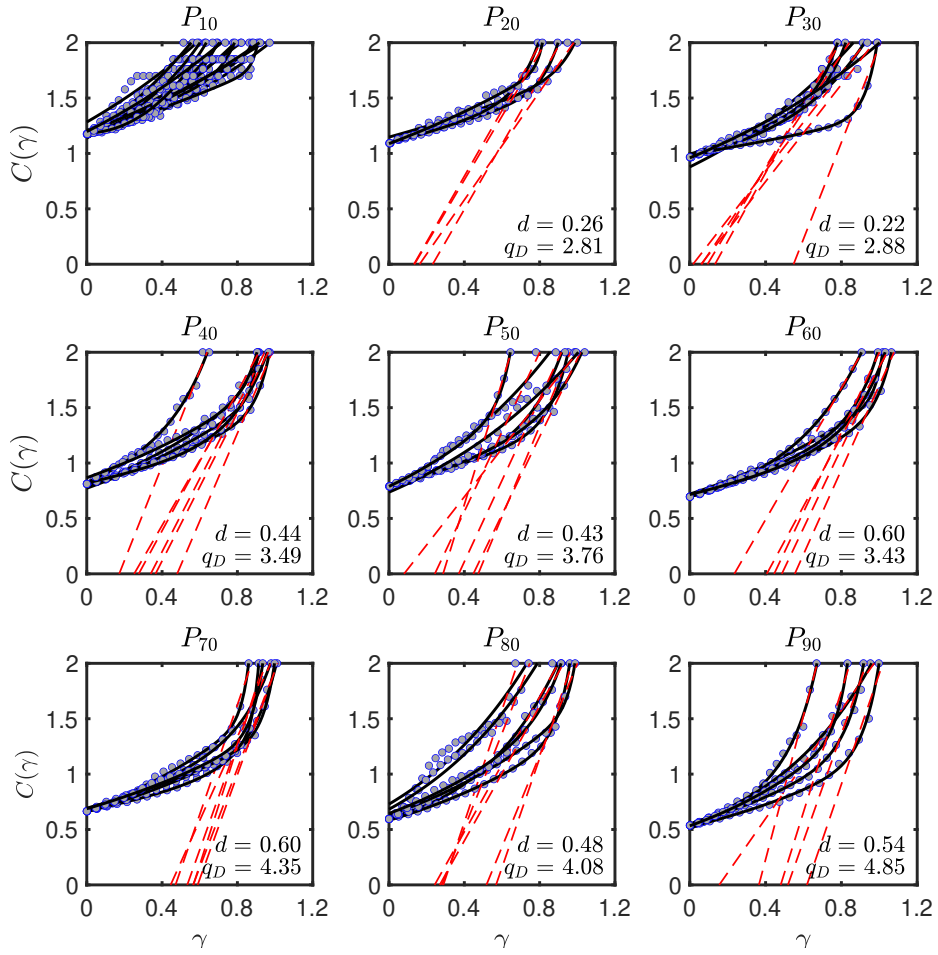


FIG. 3. Spatial codimension function for the rainfall intensities measured by the S-POL Radar (blue dots). The continuous black line is representing an exponential fitting (of the form $C(\gamma) = c_1 \exp(c_2\gamma) + c_3 \exp(c_4\gamma)$) to computed codimension function directly obtained from data. The dashed red line is representing a fitting to the function $C(\gamma) = q_d\,\gamma - d\,(q_d - 1)$ for $q > q_d$.

Similarly to the sampling dimensions, spatial codimension functions change over time as well. Spatial codimension functions present changes in their concavity which primarly depends on the number and variability of the spatial features of the rainfall intensity field. However, codimension functions of percentiles 60 and 70, which have the highest quantity and variability of rainfall intensity, exhibit some similarities in their shape and geometrical characteristics. Another way to appreciate the characteristics of the codimension function is through the sampling dimension. In general, for smaller values of D_0, the codimension function has a reduced amount of scaling exponents and its appearance is rather shrunk and there is a monotonic exponential growth in the codimension function. Clearly, the spatial structure of this rainfall intensity fields are statistically less complex, therefore, statistical moment divergence does not exist. As the sampling dimension reaches higher values than 1.0, the codimension function changes to a more complex form in which there could be a statistical moment divergence and a higher amplitude of scaling exponents in the spatial description of rainfall intensity fields. For those fields with lower values of the sampling dimension, is observed that $d \approx 0.2$ and $q_D \approx 2.8$, and for those fields with sampling dimension D_0 near to 1.3, is obtained $d \approx 0.4$ and $q_D \approx 3.8$. Recalling that mentioned above, those fields with sampling dimensions D_0 among percentiles 60 and 70 represent fields with higher variability and rainfall intensity, but they also represents the highest values of d (i.e. $d = 0.6$).

TABLE III. Estimations of the time sampling dimension D_0, the time–averaged rainfall intensity $\overline{i(x,y,t)}$ and the standard deviation of rainfall intensity $\mathrm{var}\{i(x,y,t)\}$ for the S-POL rainfall intensity time series. These estimations are classified by percentiles of the fractal dimension of every rainfall intensity time series.

Percentil	**10**	**20**	**30**	**40**	**50**	**60**	**70**	**80**	**90**	**100**
D_0	0.582	0.593	0.600	0.605	0.611	0.616	0.622	0.630	0.641	0.805
$\overline{i(x,y,t)}$	1.479	1.597	1.717	1.644	1.621	1.986	1.936	2.201	2.188	2.282
$\mathrm{var}\{i(x,y,t)\}$	5.941	6.248	6.354	6.223	6.052	6.834	6.537	7.096	7.083	7.331

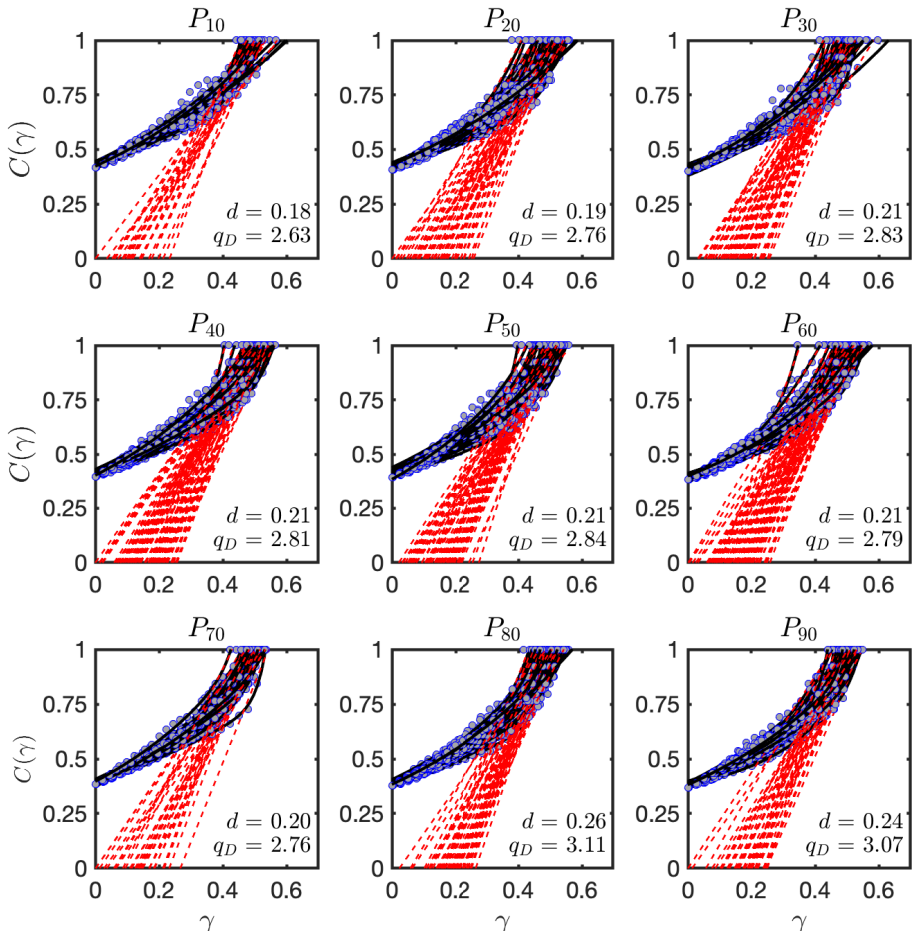


FIG. 4. Time codimension function for the rainfall intensities measured by the S-POL Radar (blue dots). The continuous black line is representing an exponential fitting (of the form $C(\gamma) = c_1 \exp(c_2\gamma) + c_3 \exp(c_4\gamma)$) to computed codimension function directly obtained from data. The dashed red line is representing a fitting to the function $C(\gamma) = q_d\,\gamma - d\,(q_d - 1)$ for $q > q_d$.

Table III exhibits a statistical summary of the sampling dimension D_0, the time–averaged rainfall intensity $\overline{i(x,y,t)}$ and the standard deviation of rainfall intensity $\mathrm{var}\{i(x,y,t)\}$. In the time domain, the sampling dimension D_0 exhibits high variability which ranges between 0.27 and 0.81 with an averaged value of 0.61. Clearly, these results suggest there could be an empirical relationship between space and time sampling dimensions. As compared both results, the time sampling dimension D_0^{time} is almost the half of the space fractal dimension D_0^{space}, i.e. $D_0^{\mathrm{time}} \approx 0.5\, D_0^{\mathrm{space}}$ (see Table IV). Although, this empirical premise is not satisfied at all, it shows a simple relation-

ship between geometrical properties of the space–time rainfall intensity field. Moreover, it induces that there could be a geometrical dependence between sampling dimensions which is modulated by the rainfall intensity in a non–linear fashion, as follows:

$$\frac{i_{\text{time}}}{i_{\text{space}}} = \phi \left[\frac{D_0^{\text{time}}}{D_0^{\text{space}}} \right]^{-\varphi} \tag{29}$$

where ϕ and φ would be regional parameters of the rainfall intensity field. As observed at Table III, either the time–averaged rainfall intensity $\overline{i(x,y,t)}$ or the standard deviation of rainfall intensity $\text{var}\{i(x,y,t)\}$ grow as D_0 increases. In time domain, the time–averaged rainfall intensity and its variability is higher than those values observed in the space domain; furthermore, time domain exhibits wider fluctuations than those observed in the space domain.

TABLE IV. Estimations of the time sampling dimension D_0, the time–averaged rainfall intensity $\overline{i(x,y,t)}$ and the standard deviation of rainfall intensity $\text{var}\{i(x,y,t)\}$ for the S-POL rainfall intensity time series. These estimations are classified by percentiles of the fractal dimension of every rainfall intensity time series.

Percentil	**10**	**20**	**30**	**40**	**50**	**60**	**70**	**80**	**90**	**100**
$D_0^{\text{time}}/D_0^{\text{space}}$	0.686	0.585	0.532	0.503	0.480	0.461	0.446	0.433	0.423	0.453
$i_{\text{time}}/i_{\text{space}}$	1.752	1.101	0.621	1.018	0.800	0.870	0.672	1.248	0.918	0.843

Figure 4 shows time codimension functions for the time domain analysis. In time domain, time series of rainfall intensity were extracted for every spatial location $\{x, y\}$ and they were classified by percentiles of their sampling dimension values. As observed at Figure 4, all time codimension functions are quite similar in shape or distribution, with no difference of its statistical classification order. Time codimension functions can be also described by exponential functions as observed in Figure 4 and these codimension functions also exhibit statistical moment divergences. As an example, for values of D_0 near to 0.61, then $d \approx 0.21$ and $q_D \approx 2.8$. It is highlighted that time and space codimension functions were also fitting to power functions but these functions exhibit a less fitting degree under the criteria of coefficients of determination.

B. Rainfall Intensity–Area Relationships

In order to understand the relationship between rainfall intensity and the area where rainfall takes place, a cluster detection algorithm was developed. This algorithm allowed to compute the cluster size distribution $f_i(A)$ of rainfall intensity i in the observational window. The cluster size distribution is here defined by $f_i(A) = n_A/N_c]_i$ where N_A is the number of clusters of size A (expressed in square kilometers) and rainfall intensity i, and N_c is the total number of clusters with rainfall intensity i. Figure 5 exhibits a plot of the cluster size distributions for some ranges of rainfall intensity. The dots in the plot are representing the empirical distribution for every cluster size group and the continuous black lines are denoting a power fitting the tail of empirical distributions. Every empirical distribution was computed for a range of rainfall intensity values. As shown in Figure 5, bigger areal extension of clusters is given in those cluster with lower rainfall intensity values, and the converse is also observed in data; smaller areal extension of clusters is identified in those with higher rainfall intensity values. Results set that tails of cluster size distributions follow a power law and it is more clear in those distributions with lower rainfall intensity values. Tail distributions for higher rainfall intensity values depicts a flat shape in our results, nonetheless, the spatial resolution of data set a restriction in the spatial description of the most intense rainfall events. Based on the results, the algebraic decay in the cluster size distributions depends on the cluster size A and its spatially–averaged rainfall intensity i. Therefore, one could suggest the following approximation:

$$f_i(A) \propto A^{m_i} \tag{30}$$

where $m_i < 0$ is an exponent depending on the rainfall intensity values of the cluster.

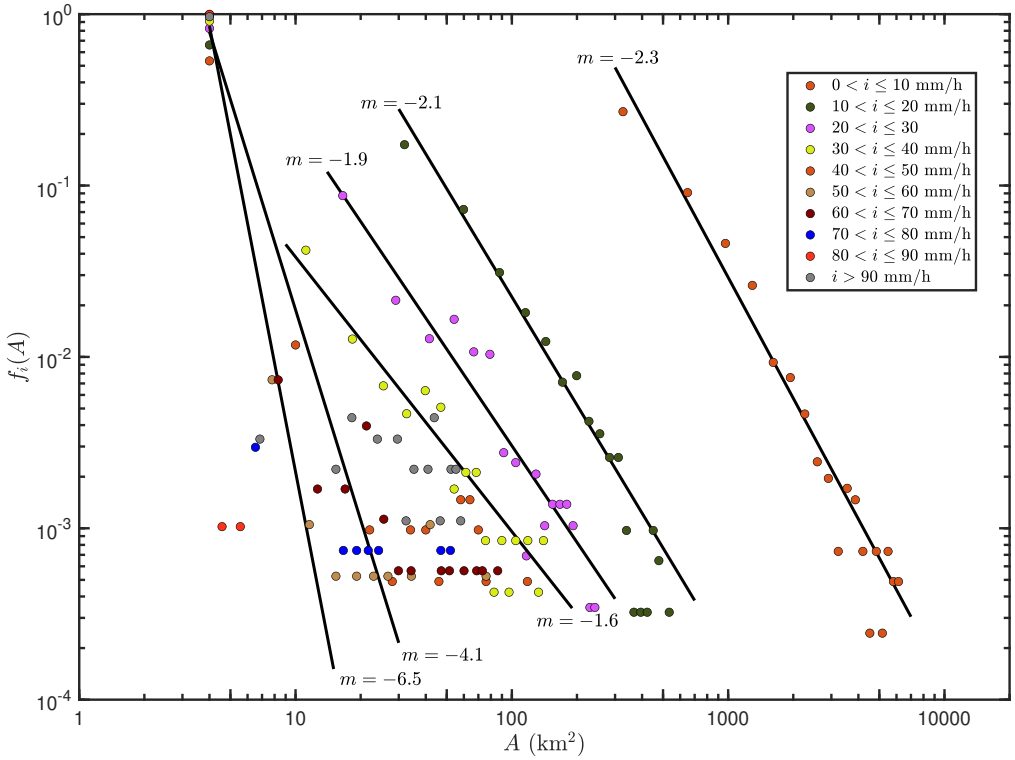


FIG. 5. Cluster size distributions of rainfall intensities measured by the S–POL Radar (coloring dots). The continuous black lines are representing a power fitting to the tails of empirical distributions.

C. Dynamic Scaling Exponents

The dynamic scaling exponent z was computed for the S–POL Radar data in order to identify a relationship between the scaling properties of the rainfall intensity field and those found in dynamic aggregation processes. Figure 6 is showing some plots of the relationship between the mean cluster size A and time duration T_d of rainfall events. Every plot in Figure 6 depicts time–averaged rainfall events for specific time duration; for instance, the upper right panel of Figure 6 is depicting a rainfall event with duration of 180 minutes (3.0 hours). On the other hand, every plot in Figure 6 shows a power fitting to a data set into the relationship T_d — A. Clearly, every rainfall event is characterized for a growth stage and a decrease stage. The power fitting was made for the growth–stage data to compute the dynamic scaling exponent z. This scaling exponent is different for every duration of the selected rainfall events and there is not a clear pattern to explain any relationship between the total time duration of the rainfall event and dynamic scaling exponent values; however, the characteristic cluster size A_i of rainfall intensity i can be approximated by:

$$A_i \propto T_d^z \tag{31}$$

and therefore, the cluster size distribution can also be approximated by:

$$f_i(A) \propto A_i^m \Phi\left(\frac{A_i}{T_d^z}\right) \propto T_d^{\psi} \tag{32}$$

where $\psi = m\,z$, is the product between the scaling exponents m and z and $\Phi(\cdot)$ is a scaling function which satisfies that $\Phi(x) \to 1$ for $x >> 1$.

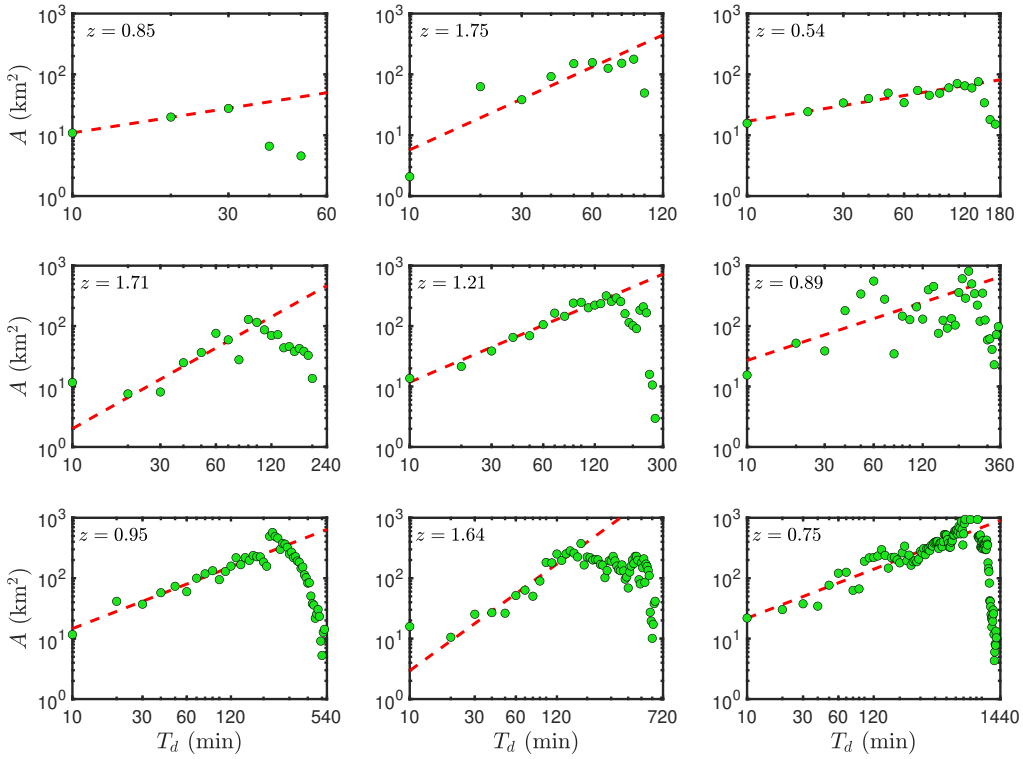


FIG. 6. Mean cluster size (in squared kilometers) with rainfall intensities less than 10 mm/h (green dots) as a function ot time duration of mean rainfall events. The duration of rainfall events that were selected are 60 min, 120 min, 180 min, 240 min, 300 min, 360 min, 540 min, 720 min and 1440 min. The upper left panel is describing a rainfall event of 60 min and the lower right panel is describing a rainfall event of 1440 min. For every panel, the dashed red lines are representing a power fitting to the relationship T_d vs A.

IV. CONCLUSIONS

In S–POL rainfall intensity fields arise fluctuations in several spatial and time scales under different scaling laws, and these facts confirms rainfall is a multi-scale phenomena where several scaling laws emerge. Although rainfall presents some similarities to dynamic aggregation processes, which are studied in critical phenomenon, it does not have universal scaling exponents and many factors contribute in the setting of their scaling exponents. In the light of our results, IADF relationship could be parameterized as follows:

$$i_\lambda = C_o \left[\frac{T_r}{T_d^{1+d\,(q_d-1)}}\right]^{\frac{1}{q_d}}; \qquad A_i \approx C_3 \left[\frac{T_r}{i_\lambda^{q_d}}\right]^{\gamma}; \qquad f_i(A) = C_2\, T_d^{\psi}; \tag{33}$$

where,

$$\gamma = \frac{z}{1+d\,(q_d-1)} \tag{34}$$

is a composed dynamic scaling exponent for the IADF relationship. The parsimonious mathematical structure of the IADF relationship, exhibited above in equation 33, ease the analysis and design

of hydraulic structures and some others engineering applications, nonetheless, the main constrain in the use of this model is to have into account that in the rainfall complexity arises non–universal dynamic scaling exponents, whereby it is necessary to know in advance the basics assumptions in the parameters definition.

AUTHOR CONTRIBUTIONS

Victor Peñaranda (V.P.) & David Serrano (D.S.) conceived the research, V.P. generated all figures, D.S. & Mahesh Maskey (M.M.) collected and processed data, D.S. and M.M. coded some algorithms in Python, V.P. coded some algorithms in MATLAB, and all authors contributed to writing the manuscript and interpreting the results.

DATA AND CODE AVAILABILITY

Data and codes to reproduce the results presented here is available at: `https://github.com/mlmaskey/IDFCurves`

DECLARATION OF INTERESTS

The authors declare no competing interests.

[1] Bendjoudi, H.; Hubert, P.; Schertzer, D.; Lovejoy, S. Interprétation multifractale des courbes intensité-durée-fréquence des précipitations. *Comptes Rendus de l'Académie des Sciences - Series IIA - Earth and Planetary Science*, **1997**, *325:5*, 323–326.

[2] Bernard, M. Formulas for rainfall intensities of long duration. Transactions of the American Society of Civil Engineers, **1932**, *96*, 592–606.

[3] Castro, J.; Carsteanu, A.A.; Flores, C.G. Intensity–duration–area–frequency functions for precipitation in a multifractal framework. *Physica A*, **2004**, *338*, 206–210.

[4] Ceresetti, D. Structure spatio-temporelle des fortes précipitations: Applicatio á la région Cévennes Vivarais, *Ph.D. thesis*, **2011**, Université de Grenoble,

[5] Davies, D. L.; Bouldin, D. W. A Cluster Separation Measure. *IEEE Transactions on Pattern Analysis and Machine Intelligence*, **1979**, *PAMI-1 (2)*, 224–227.

[6] De Michelle, C; Kottegoda, N; Rosso, R. IDAF (intensity-duration-area frequency) curves of extreme storm rainfall: a scaling approach. *Water Science Technology*, **2002**; *45:2*, 83–90.

[7] De Michelle, C.; Zenoni, E.; Pecora, S.; Rosso, R. Analytical derivation of rain intensity–duration–area–frequency relationships from event maxima. *Journal of Hydrology*, **2011**; *399*, 385–393.

[8] Deutsch, A.; Dormann, S. *Growth Processes*. In: Cellular Automaton Modeling of Biological Pattern Formation. Modeling and Simulation in Science, Engineering and Technology. Birkhäuser Boston, 2005; pp. 129–142.

[9] Feder, J. *Fractals*; Plenum Press: New York - London, 1988; pp. 66–96.

[10] Hubert, P.; Bendjoudi, H.; Schertzer, D.; Lovejoy, S. A multifractal explanation for rainfall intensity–duration–frequency curves. Heavy Rain and Flash Floods, Istanbul Technical University, 1998, pp. 21–28.

[11] Hubert, P.; Tessier, Y.; Lovejoy, S.; Schertzer, D.; Schmitt, F.; Ladoy, P.; Carbonnel, J. P.; Violette, S.; Desurosne, I. Multifractals and extreme rainfall events. *Geophysical Research Letters*, **1993**, *20:10*, 931–934.

[12] Langousis, A; Veneziano, D. Intensity–duration–frequency curves from scaling representations of rainfall. *Water Resources Research*, **2007**, *43:W02422*, 1–12.

[13] Lovejoy, S.; Schertzer, D. Multifractals and rain. In Z. Kundzewicz (Ed.), New Uncertainty Concepts in Hydrology and Water Resources (International Hydrology Series, pp. 61-103). Cambridge: Cambridge University Press. 1995.
[14] Lovejoy, S.; Schertzer, D. *The Weather and Climate: Emergent Laws and Multifractal Cascades*; Cambridge University Press: Cambridge, UK, 2013; pp. 1–424.
[15] Mélèse, V.; Blanchette, J.; Creutin, J.D. A Regional Scale-Invariant Extreme Value Model of Rainfall Intensity-Duration–Area–Frequency Relationships. *Water Resources Research*, **2019**, *55*, 1–20.
[16] Mesa, O.; Peñaranda, V. Complejidad de la estructura espacio–temporal de la precipitación. *Rev. Acad. Colomb. Cienc. Ex. Fis. Nat.*, **2015**, *39:152*, 304–320.
[17] Panthou, G.; Vischel, T.; Lebel, T,; Quantin, G.; Molinié, G. Characterising the space–time structure of rainfall in the Sahel with a view to estimating IDAF curves. *Hydrol. Earth Syst. Sci.*, **2014**, *18*, 5093–5107.
[18] Peñaranda, V. Looking for a physical basis of rainfall multifractality. *Ph.D. Thesis*, **2020**, Universidad Nacional de Colombia, Medellin, CO.
[19] Raudkivi, A. *Hydrology*; Pergamon Press: Toronto, CA, 1979.
[20] Sherman, C. Frequency and intensity of excessive rainfalls at Boston, Massachusetts. Transactions of the American Society of Civil Engineers, **1931**, *95*, 951–960.
[21] Schertzer, D.; Lovejoy, S. Singularités, anisotropes, divergence des moments en turbulence: invariance de'échelle généralisée et processus multiplicatifs. *Annales des sciences mathématiques du Québec*, **1987**, *2:1*, 139–181.
[22] Tessier, Y.; Lovejoy, S.; Hubert, P.; Schertzer, D.; Pecknold, S. Multifractal analysis and modeling of rainfall and river flows and scaling, causal transfer functions. *Journal of Geophysical Research: Atmospheres*, **1996**, *101:D21*, 26427–26440.
[23] Witten, T. A.; Sander, L. M. Diffusion–Limited Aggregation, a Kinetic Critical Phenomenon. *Phys. Rev. Lett.*, **1981**, *47:19*, 1400–1403.
[24] Veneziano, D.; Furcolo, P. Multifractality of rainfall and scaling of intensity-duration-frequency curves. *Water Resources Research*, **2002**, *38:12*, 42-1–42-12.
[25] Veneziano, D.; Langousis, A.; Furcolo, P. Multifractality and rainfall extremes: A review. *Water Resources Research*, **1993**, *42:6*, 1–18.
[26] Vicsek, T.; Family, F. Dynamic scaling for aggregation of clusters. *Physical Review Letters*, **1984**, *52:19*, 1669–1672.

Supplemental Material

Appendix A: Multifractal Scaling

Being **R** a rainfall field whose fluctuation are defined as measures $\{\mu_i\}$, it will be multifractal if there exists a range of scaling exponents $A = (\alpha_{min}, \alpha_{max})$ defined on a fractal set whose dimension $f(\alpha)$ depends on α. As the scale $\lambda \to 0$, the rainfall fluctuations $\{\mu_i\}$ satisfy the following power-law relationship: $\mu_\alpha \sim \lambda^\alpha$, where α-exponents are known as singularity exponents of order α and the function $f(\alpha)$ is known as the *multifractal spectrum* of the rainfall fluctuations $\{\mu_i\}$ [9, 25]. Moreover, the probability density function $f_\mu(\mu(\lambda))$ of the (random) measures $\{\mu_i(\lambda)\}$, defined on **R** at the scale λ, allows to compute statistical moments of these measures as follows:

$$M_\mu^q(\lambda) = \int \mu^q(\lambda) f_\mu(\mu(\lambda))\, d\mu = \mathrm{E}[\mu^q(\lambda)] \tag{A1}$$

Being $\lambda^{d-f(\alpha)}$ the probability of having $\mu_\alpha \sim \lambda^\alpha$, i.e. the probability of a ball at the scale λ of being into the set $\mathscr{C}_\alpha$ with dimension $f(\alpha)$ and Euclidean embedding dimension d, the power–law relationship $\mu_\alpha \sim \lambda^\alpha$ re-defines the statistical moments of rainfall fluctuations as follows:

$$M_\mu^q(\lambda) = \int \lambda^{\alpha\, q + d - f(\alpha)} d\mu = \int \lambda^{\alpha\, q + C(\alpha)} d\mu \tag{A2}$$

where $C(\alpha) = d - f(\alpha)$ is called the co-dimension function. When $\lambda \to 0$ at equation A2, the smallest exponents of the power law into the integral dominate; therefore:

$$M_\mu^q(\lambda) \propto \lambda^{\theta_q} \qquad \text{as} \quad \lambda \to 0 \tag{A3}$$

where $\theta_q = \inf_\alpha [q\,\alpha + d - f(\alpha)]$ is the moment scaling function and it is also related to the function $f(\alpha)$ through a Legendre transformation as follows:

$$\theta_q = \inf_\alpha \{q\,\alpha + d - f(\alpha)\} \tag{A4}$$

$$f(\alpha) = \inf_\alpha \{q\,\alpha + d - \theta_q\} \tag{A5}$$

In the context of *Universal Multifractals*, some scaling relations have also been derived for the exceedance probability of multifractal measures [10, 11, 13, 14]. If now it is considered the average measure density ϵ_λ at the scale λ, the probability of having $\epsilon_\lambda > \lambda^\gamma$ is $\lambda^{-C(\gamma)}$, where $C(\gamma) = d - f(\alpha)$ is the codimension function of ϵ_λ (or exponent that measure the fraction of the space occupied by the set defined by $\{\epsilon_\lambda > \lambda^\gamma\}$) and γ is a local singularity exponent. Following the above definition and as $\lambda \to \infty$, the statistical moments of ϵ_λ is given by:

$$M_\epsilon^q(\lambda) \propto \lambda^{K(q)} \qquad \text{as} \quad \lambda \to \infty \tag{A6}$$

where $K(q) = \sup_\gamma \{q\,\gamma - C(\gamma)\}$ is the moment scaling function and it is also related to $C(\gamma)$ through the following Legendre transformation:

$$K(q) = \sup_\gamma \{q\,\gamma - C(\gamma)\} \tag{A7}$$

$$C(\gamma) = \sup_\gamma \{q\,\gamma - K(q)\} \tag{A8}$$

The codimension function $C(\gamma)$ is a statistical scaling exponent that characterizes how the probability changes with the scale; moreover, if the moment scaling function $K(q)$ has a non–linear behavior, the average measure densities are recognized as multifractal measures. The codimension function $C(\gamma)$ is an increasing monotone function $dC(\gamma)/d\gamma > 0$; besides, when its derivative is evaluated at γ_1, i.e. the singularity associated to the mean (at the order of the moment $q = 1$), then $dC(\gamma_1)/d\gamma = 1$; therefore, $C(\gamma_1) \equiv C_1 = \gamma_1 = dK(q = 1)/dq$.